Dependence of fusion on isospin dynamics

K. Godbey,[1,*] A.S. Umar,[1,†] and C. Simenel[2,‡]

[1]*Department of Physics and Astronomy, Vanderbilt University, Nashville, TN 37235, USA*
[2]*Department of Nuclear Physics, Research School of Physics and Engineering, The Australian National University, Canberra ACT 2601, Australia*

(Dated: September 29, 2016)

We introduce a new microscopic approach to calculate the dependence of fusion barriers and cross-sections on isospin dynamics. The method is based on the time-dependent Hartree-Fock theory and the isoscalar and isovector properties of the energy density functional (EDF). The contribution to the fusion barriers originating from the isoscalar and isovector parts of the EDF is calculated. It is shown that for non-symmetric systems the isovector dynamics influence the sub-barrier fusion cross-sections. For most systems this results in an enhancement of the sub-barrier cross-sections, while for others we observe differing degrees of hindrance. We use this approach to provide an explanation of recently measured fusion cross sections which show a surprising enhancement at low $E_{\rm c.m.}$ energies for the system ^{40}Ca+^{132}Sn as compared to the more neutron-rich system ^{48}Ca+^{132}Sn, and discuss the dependence of sub-barrier fusion cross-sections on transfer.

arXiv:1609.08698v1 [nucl-th] 27 Sep 2016

One of the major open questions in fusion reactions of exotic neutron-rich nuclei is the dependence of the fusion cross section on the neutron excess, or equivalently on the total isospin quantum number $T_z = (Z-N)/2$. This is a timely subject given the expected availability of increasingly exotic beams at rare isotope facilities [1]. The influence of isospin dynamics on fusion is also one of the key questions pertaining to the production of superheavy elements using neutron rich nuclei [2]. Besides being a fundamental nuclear structure and reaction question, the answer to this inquiry is also vital to our understanding of the nuclear equation of state (EOS) and symmetry energy [3]. The EOS plays a key role in elucidating the structure of exotic nuclei [4], the dynamics of heavy ion collisions [5,6], the composition of neutron stars [7–10], and the mechanism of core-collapse supernovae [11–13]. The influence of isospin flow during heavy-ion reaction is usually discussed in term of the (N/Z) asymmetry of the target and projectile or the Q-values for neutron transfer. Dynamically, (N/Z) asymmetry leads to the so-called pre-equilibrium giant-dipole resonance (GDR), which has been studied using various dynamical approaches [14–22]. The main issue with these microscopic calculations is that it is often difficult, if not impossible, to quantitatively assess the influence of the GDR on fusion cross-sections. Other approaches have also been considered to study the impact of neutron transfer on fusion barriers and fusion cross-sections. These include the coupled-channels (CC) approach [23–25] and models incorporating intermediate neutron rearrangements [26–28].

The predictions of fusion enhancement based on Q-value arguments have been recently challenged by a series of experiments carried out with radioactive ^{132}Sn beams and with stable ^{124}Sn beams on ^{40,48}Ca targets [29]. It turns out that the ^{40}Ca+Sn systems have many positive Q-values for neutron-pickup while all the Q-values for ^{48}Ca+Sn are negative. However, the data analysis reveals that the fusion enhancement is not proportional to the magnitudes of those Q-values. Particularly puzzling is the experimental observation of a sub-barrier fusion enhancement in the system ^{40}Ca+^{132}Sn as compared to the more neutron-rich ^{48}Ca+^{132}Sn system. Part of the puzzle comes from the fact that the 8 additional neutrons in ^{48}Ca should increase the attractive strong nuclear interaction and thus lower the fusion barrier, resulting in an enhanced sub-barrier fusion cross section. One explanation is that the dynamics will "wash out" the static structure effects such as the Coulomb barrier lowering due to neutron skin [30]. This anomaly was also studied in a recent experiment [31].

In this work we address the impact of isospin dynamics on fusion barriers and cross-sections using the microscopic time-dependent Hartree-Fock (TDHF) theory [32,33] together with the density-constrained TDHF (DC-TDHF) method for calculating fusion barriers [34]. In the TDHF approximation the many-body wavefunction is replaced by a single Slater determinant and this form is preserved at all times, implying that two-body correlations are neglected. In this limit, the variation of the time-dependent action with respect to the single-particle states, ϕ^*_λ, yields the most probable time-dependent path in the multi-dimensional space-time phase space represented as a set of coupled, nonlinear, self-consistent initial value equations for the single-particle states

$$h(\{\phi_\mu\})\,\phi_\lambda(r,t) = i\hbar\frac{\partial}{\partial t}\phi_\lambda(r,t) \quad (\lambda = 1,...,A)\,, \qquad (1)$$

where h is the HF single-particle Hamiltonian. These are the fully microscopic time-dependent Hartree-Fock equations.

Almost all TDHF calculations employ the Skyrme EDF, which allows the total energy of the system to be represented as an integral of the energy density $\mathscr{H}(\mathbf{r})$ [35]

$$E = \int d^3\mathbf{r}\,\mathscr{H}(\mathbf{r})\,, \qquad (2)$$

which includes the kinetic, isoscalar, isovector, and Coulomb terms [36]:

$$\mathscr{H}(\mathbf{r}) = \frac{\hbar^2}{2m}\tau_0 + \mathscr{H}_0(\mathbf{r}) + \mathscr{H}_1(\mathbf{r}) + \mathscr{H}_C(\mathbf{r})\,. \qquad (3)$$

In particular,

$$\mathscr{H}_{\rm I}(\mathbf{r}) = C_{\rm I}^{\rho}\rho_{\rm I}^2 + C_{\rm I}^{s}\mathbf{s}_{\rm I}^2 + C_{\rm I}^{\Delta\rho}\rho_{\rm I}\Delta\rho_{\rm I} + C_{\rm I}^{\Delta s}\mathbf{s}_{\rm I}\cdot\Delta\mathbf{s}_{\rm I} + C_{\rm I}^{\tau}\left(\rho_{\rm I}\tau_{\rm I} - \mathbf{j}_{\rm I}^2\right) + C_{\rm I}^{T}\left(\mathbf{s}_{\rm I}\cdot\mathbf{T}_{\rm I} - \overleftrightarrow{J}_{\rm I}^2\right) + C_{\rm I}^{\nabla J}\left(\rho_{\rm I}\nabla\cdot\mathbf{J}_{\rm I} + \mathbf{s}_{\rm I}\cdot(\nabla\times\mathbf{j}_{\rm I})\right), \quad (4)$$

where we have used the gauge invariant form suitable for time-dependent calculations. The isospin index $\mathrm{I} = 0, 1$ for isoscalar and isovector energy densities, respectively. The most common choice of Skyrme EDF restricts the density dependence of the coupling constants to the $C_{\rm I}^{\rho}$ and $C_{\rm I}^{s}$ terms only. These density dependent coefficients induce the coupling of isoscalar and isovector fields in the Hartree-Fock Hamiltonian. The isoscalar (isovector) energy density, $\mathscr{H}_0(\mathbf{r})$ ($\mathscr{H}_1(\mathbf{r})$), depends on the isoscalar (isovector) particle density, $\rho_0 = \rho_n + \rho_p$ ($\rho_1 = \rho_n - \rho_p$), with analogous expressions for other densities and currents. Values of the coupling coefficients as well as their relation to the alternative parametrizations of the Skyrme EDF can be found in [36].

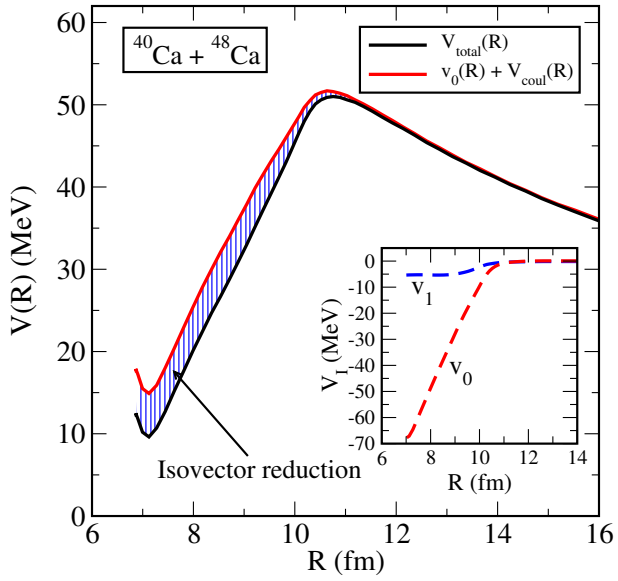

FIG. 1. (Color online) For the ^{40}Ca+^{48}Ca system; Total and isoscalar DC-TDHF potentials. The shaded region corresponds to the reduction originating from the isovector contribution to the energy density. The insert shows the isoscalar and isovector contributions to the interaction barrier without the Coulomb potential. The TDHF collision energy was $E_{\rm c.m.} = 55$ MeV.

The above form of the EDF is more suitable for studying the isospin dependence of nuclear properties and have been employed in nuclear structure studies [36]. In the same spirit we can utilize this approach to study isospin dependent effects in nuclear reactions microscopically. In particular, the density-constrained time-dependent Hartree-Fock (DC-TDHF) method [34] can be employed to study isospin effects on fusion barriers and fusion cross-sections. The DC-TDHF approach calculates the nucleus-nucleus potentials $V(R)$ directly from TDHF dynamics and has been used to calculate fusion cross-sections for a wide range of reactions [37–43]. The basic idea of this approach is the following: At certain times t or, equivalently, at certain internuclear distances $R(t)$, a static energy minimization is performed while constraining the proton and neutron densities to be equal to the instantaneous TDHF densities. We refer to the minimized energy as the "density constrained energy" $E_{\rm DC}(R)$. The ion-ion interaction potential $V(R)$ is obtained by subtracting the constant binding energies $E_{\rm A_1}$ and $E_{\rm A_2}$ of the two individual nuclei

$$V(R) = E_{\rm DC}(R) - E_{\rm A_1} - E_{\rm A_2}\ . \quad (5)$$

The calculated ion-ion interaction barriers contain all of the dynamical changes in the nuclear density during the TDHF time-evolution in a self-consistent manner. As a consequence of the dynamics the DC-TDHF potential is energy dependent [37]. Using the decomposition of the Skyrme EDF into isoscalar and isovector parts [Eq. (4)], we can re-write this potential as

$$V(R) = \sum_{\rm I=0,1} v_{\rm I}(R) + V_C(R)\,, \quad (6)$$

where $v_{\rm I}(R)$ denotes the potential computed by using the isoscalar and isovector parts of the Skyrme EDF given in Eq. (3) in Eq. (5). The Coulomb potential is also calculated via Eq. (5) using the Coulomb energy density.

We have used the DC-TDHF approach to study fusion barriers for a number of systems. Calculations were done in a three-dimensional Cartesian geometry with no symmetry assumptions [44] and using the Skyrme SLy4 EDF [45]. The three-dimensional Poisson equation for the Coulomb potential is solved by using Fast-Fourier Transform techniques and the Slater approximation is used for the Coulomb exchange term. The box size used for all the calculations was chosen to be $60\times30\times30$ fm^3, with a mesh spacing of 1.0 fm in all directions. These values provide very accurate results due to the employment of sophisticated discretization techniques [46].

In Fig. 1 we show the total and isoscalar fusion barriers (both including the Coulomb contribution) for the ^{40}Ca+^{48}Ca system at $E_{\rm c.m.} = 55$ MeV. For the Ca+Ca systems the energy dependence is relatively weak [37,47,48]. The reduction of the isoscalar barrier is due to the isovector contribution. It is evident that the isovector dynamics results in the narrowing of the fusion barrier, thus resulting in an enhancement of the sub-barrier fusion cross-sections. The insert in Fig. 1 shows the isovector and isoscalar components without the Coulomb contribution. We have also calculated fusion barriers for the ^{40}Ca+^{40}Ca and ^{48}Ca+^{48}Ca systems, where the isovector contribution is zero as expected from symmetry.

As an example of a more asymmetric system we performed calculations for the ^{16}O+^{208}Pb system at $E_{\rm c.m.} = 75$ MeV. Results are shown in Fig. 2(a). Here we see a substantial enhancement of sub-barrier fusion due to the isovector dynamics. For this system we have performed further calculations at c.m. energies of 90 MeV and 120 MeV shown in Fig. 2(b-c).

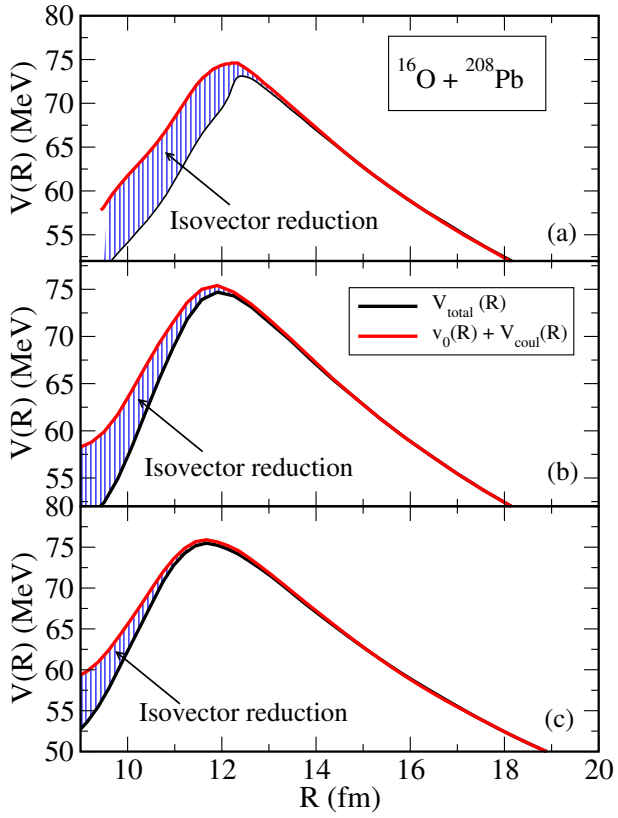

FIG. 2. (Color online) For the ^{16}O+^{208}Pb system; (a) Total and isoscalar DC-TDHF potentials at $E_{\rm c.m.} = 75$ MeV. The shaded region corresponds to the reduction originating from the isovector contribution to the energy density. (b) Same as in (a) except for $E_{\rm c.m.} = 90$ MeV. (c) Same as in (a) except for $E_{\rm c.m.} = 120$ MeV.

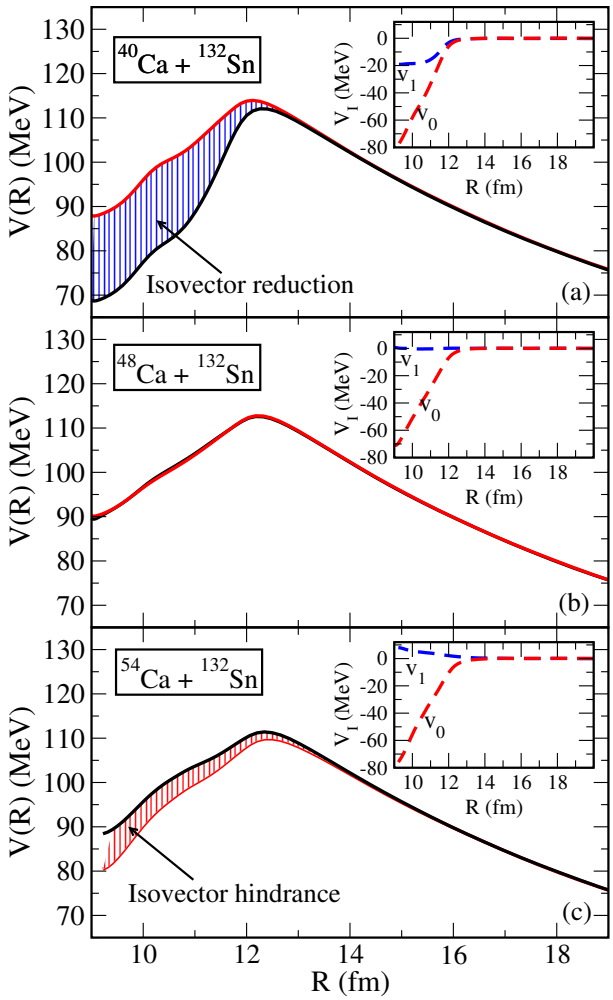

FIG. 3. (Color online) For (a) ^{40}Ca+^{132}Sn, (b) ^{48}Ca+^{132}Sn, (c) ^{54}Ca+^{132}Sn systems; Total and isoscalar DC-TDHF potentials. In (a) the blue shaded region corresponds to the reduction originating from the isovector contribution. In (b) we see no isovector effect. In (c) the isovector effect is reversed causing hindrance as shown by the red shaded region. The inserts show the isoscalar and isovector contributions to the interaction barrier without the Coulomb potential. The TDHF collision energy was $E_{\rm c.m.} = 120$ MeV.

As the beam energy increases, the relative contribution from the isovector component to the total barrier decreases, while the overall barrier height increases with increasing energy. At TDHF energies much higher than the barrier height the total barriers approaches the frozen density barrier [37,48] due to the inability of the system to rearrange at that time-scale at which time the isovector contribution vanishes as well. The above results demonstrate the influence of isovector dynamics on typical fusion barriers.

We next look at Ca+Sn reactions. The experimental observation of a sub-barrier fusion enhancement in the system ^{40}Ca+^{132}Sn as compared to more neutron-rich system ^{48}Ca+^{132}Sn was the subject of a previous DC-TDHF study [49], where it was shown that the fusion barriers for the two systems have essentially the same height but the fusion barrier for the ^{48}Ca+^{132}Sn system was much wider than that for the ^{40}Ca+^{132}Sn system. We see in Fig. 3(a) a strong reduction of the isoscalar barrier due to the isovector contribution. This behavior is similar to that of the previous two systems albeit the isovector reduction is somewhat larger as shown in the insert of Fig. 3(a). We then performed the same calculation for the ^{48}Ca+^{132}Sn system as shown in Fig. 3(b). The startling result is the vanishing of the isovector contribution. With no isovector reduction the fusion barrier for this system is much wider than that for the ^{40}Ca+^{132}Sn system for which substantial reduction occurs. The absence of the isovector component for the ^{48}Ca+^{132}Sn system could be a reflection of the negative $Q-$values for neutron pickup. This is the first direct observation of this phenomena in TDHF calculations. This may also explain why for the ^{48}Ca+^{132}Sn system simply considering the 2^+ and 3^- excitations of the target and projectile in coupled-channel calculations is able to reproduce the sub-barrier fusion cross-sections, whereas doing the same for the ^{40}Ca+^{132}Sn system grossly under-predicts the cross-sections. In Ref. [29], this was attributed to the presence of significant transfer, which manifests itself in the isovector dynamics. In Fig. 3(c) we have also calculated the potential barriers for the theoretical ^{54}Ca+^{132}Sn reaction. Here, we see that the influ-

ence of the isovector component is reversed, as indicated by the shaded region. This reversal leads to the widening of the potential barrier, further hindering sub-barrier fusion.

In order to investigate the role of transfer in more detail we have plotted the microscopic TDHF neutron and proton currents for both systems in Fig. 4, for the same collision energy used to calculate the barriers shown in Fig. 3 and at the nuclear separation $R = 11.5$ fm, which is slightly inside the barrier but still corresponds to an early stage of the reaction. Examination of these currents shows that for the ^{40}Ca+^{132}Sn system neutrons flow from ^{132}Sn to ^{40}Ca, whereas the proton flow is from ^{40}Ca to ^{132}Sn. Proton flow for the ^{48}Ca+^{132}Sn system is similar, namely from ^{48}Ca to ^{132}Sn. However, we observe an interesting difference for the neutron flow in the ^{48}Ca+^{132}Sn system, namely a bi-directional flow between the two systems. The dynamics of this bi-directional flow results in an isovector current density in the neck region to be an order of magnitude lower for the ^{48}Ca+^{132}Sn system in comparison to the ^{40}Ca+^{132}Sn. This is the primary cause for the disappearance of the isovector contribution to the barrier. In the neck region, the relative magnitude of the proton current density of ^{48}Ca+^{132}Sn system is 30%-50% smaller than the proton current density of the ^{40}Ca+^{132}Sn. This behavior is prevalent during the entire neck dynamics. Examination of the currents for the ^{54}Ca+^{132}Sn reaction reveals that there is essentially no through-flow of neutrons or protons during the neck formation.

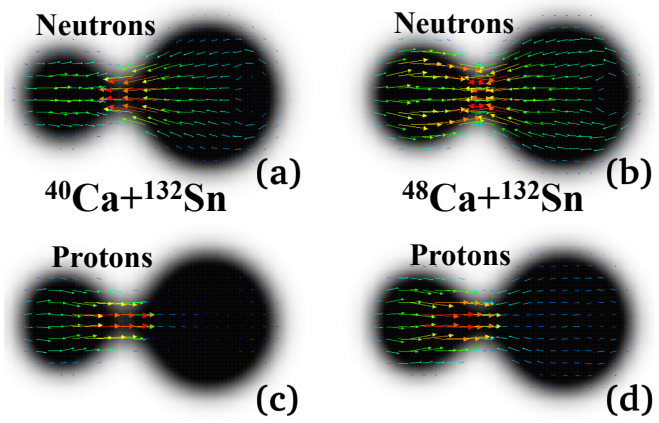

FIG. 4. (Color online) Neutron and proton current vectors in ^{40,48}Ca+^{132}Sn at $E_{\rm c.m.} = 120$ MeV and at a separation $R = 11.5$ fm between the fragments.

In summary, we have developed a microscopic approach to study the effect of isospin dynamics on fusion barriers. We have shown that for most systems isovector dynamics results in the thinning of the barrier thus enhancing the sub-barrier fusion cross-sections. The isovector reduction effect vanishes for symmetric systems as well as the ^{48}Ca+^{132}Sn system for which neutron pickup $Q-$values are all negative. These results provide a quantitative measure for the importance of transfer for sub-barrier fusion reactions. Furthermore, they elucidate the non-trivial dependence of sub-barrier fusion for neutron-rich systems and illustrate the importance of dynamical microscopic models that incorporate the nuclear structure and reactions on the same footing. A more detailed study including cross-section ratios and other systems will be the subject of a future study.

We thank K. Vo-Phuoc for useful discussions regarding the Ca+Sn systems. This work has been supported by the U.S. Department of Energy under grant No. DE-SC0013847 with Vanderbilt University and by the Australian Research Council Grant No. FT120100760,

* kyle.s.godbey@vanderbilt.edu
† umar@compsci.cas.vanderbilt.edu
‡ cedric.simenel@anu.edu.au

[1] A. B. Balantekin, J. Carlson, D. J. Dean, G. M. Fuller, R. J. Furnstahl, M. Hjorth-Jensen, R. V. F. Janssens, Bao-An Li, W. Nazarewicz, F. M. Nunes, W. E. Ormand, S. Reddy, and B. M. Sherrill, Mod. Phys. Lett. A **29**, 1430010 (2014).
[2] W. Loveland, Phys. Rev. C **76**, 014612 (2007).
[3] Bao-An Li, Àngels Ramos, Giuseppe Verde, and Isaac Vidaña, Eur. Phys. J. A **50**, 1 (2014).
[4] Wei-Chia Chen and J. Piekarewicz, Phys. Rev. C **90**, 044305 (2014).
[5] Paweł Danielewicz, Roy Lacey, and William G. Lynch, Science **298**, 1592 (2002).
[6] M. B. Tsang, Yingxun Zhang, P. Danielewicz, M. Famiano, Zhuxia Li, W. G. Lynch, and A. W. Steiner, Phys. Rev. Lett. **102**, 122701 (2009).
[7] P. Haensel and J. L. Zdunik, Astron. Astrophys. **229**, 117 (1990).
[8] Nicolas Chamel and Pawel Haensel, Living Rev. Relat. **11**, 10 (2008).
[9] C. J. Horowitz, M. A. Pérez-García, and J. Piekarewicz, Phys. Rev. C **69**, 045804 (2004).
[10] R. Utama, J. Piekarewicz, and H. B. Prosper, Phys. Rev. C **93**, 014311 (2016).
[11] P. Bonche and D. Vautherin, Nucl. Phys. A **372**, 496 (1981).
[12] Gentaro Watanabe, Hidetaka Sonoda, Toshiki Maruyama, Katsuhiko Sato, Kenji Yasuoka, and Toshikazu Ebisuzaki, Phys. Rev. Lett. **103**, 121101 (2009).
[13] G. Shen, C. J. Horowitz, and S. Teige, Phys. Rev. C **83**, 035802 (2011).
[14] C. H. Dasso, S. Landowne, and A. Winther, Nucl. Phys. A **432**, 495 (1985).
[15] Ph. Chomaz, M. Di Toro, and A. Smerzi, Nucl. Phys. A **563**, 509 (1993).
[16] V. Baran, M. Colonna, M. Di Toro, A. Guarnera, and A. Smerzi, Nucl. Phys. A **600**, 111 (1996).
[17] V. Baran, C. Rizzo, M. Colonna, M. Di Toro, and D. Pierroutsakou, Phys. Rev. C **79**, 021603 (2009).
[18] V. Baran, M. Colonna, V. Greco, and M. Di Toro, Phys. Rep. **410**, 335 (2005).
[19] V. Baran, D. M. Brink, M. Colonna, and M. Di Toro, Phys. Rev. Lett. **87**, 182501 (2001).
[20] C. Simenel, Ph. Chomaz, and G. de France, Phys. Rev. Lett. **86**, 2971 (2001).
[21] C. Simenel, Ph. Chomaz, and G. de France, Phys. Rev. C **76**, 024609 (2007).
[22] Kazuyuki Sekizawa and Kazuhiro Yabana, Phys. Rev. C **88**,

014614 (2013).
[23] N. Rowley, I. J. Thompson, and M. A. Nagarajan, Phys. Lett. B **282**, 276 (1992).
[24] Kouichi Hagino and Noboru Takigawa, Prog. Theo. Phys. **128**, 1001 (2012).
[25] D. Bourgin, C. Simenel, S. Courtin, and F. Haas, Phys. Rev. C **93**, 034604 (2016).
[26] V. I. Zagrebaev, Phys. Rev. C **67**, 061601 (2003).
[27] V. I. Zagrebaev, V. V. Samarin, and Walter Greiner, Phys. Rev. C **75**, 035809 (2007).
[28] A. V. Karpov, V. A. Rachkov, and V. V. Samarin, Phys. Rev. C **92**, 064603 (2015).
[29] J. J. Kolata, A. Roberts, A. M. Howard, D. Shapira, J. F. Liang, C. J. Gross, R. L. Varner, Z. Kohley, A. N. Villano, H. Amro, W. Loveland, and E. Chavez, Phys. Rev. C **85**, 054603 (2012).
[30] K. Vo-Phuoc, C. Simenel, and E. C. Simpson, Phys. Rev. C **94**, 024612 (2016).
[31] J. F. Liang, J. M. Allmond, C. J. Gross, P. E. Mueller, D. Shapira, R. L. Varner, M. Dasgupta, D. J. Hinde, C. Simenel, E. Williams, K. Vo–Phuoc, M. L. Brown, I. P. Carter, M. Evers, D. H. Luong, T. Ebadi, and A. Wakhle, Phys. Rev. C **94**, 024616 (2016).
[32] J. W. Negele, Rev. Mod. Phys. **54**, 913 (1982).
[33] Cédric Simenel, Eur. Phys. J. A **48**, 152 (2012).
[34] A. S. Umar and V. E. Oberacker, Phys. Rev. C **74**, 021601 (2006).
[35] Y. M. Engel, D. M. Brink, K. Goeke, S. J. Krieger, and D. Vautherin, Nucl. Phys. A **249**, 215 (1975).
[36] J. Dobaczewski and J. Dudek, Phys. Rev. C **52**, 1827 (1995).
[37] A. S. Umar, C. Simenel, and V. E. Oberacker, Phys. Rev. C **89**, 034611 (2014).
[38] C. Simenel, R. Keser, A. S. Umar, and V. E. Oberacker, Phys. Rev. C **88**, 024617 (2013).
[39] A. S. Umar, V. E. Oberacker, and C. J. Horowitz, Phys. Rev. C **85**, 055801 (2012).
[40] A. S. Umar and V. E. Oberacker, Phys. Rev. C **74**, 061601 (2006).
[41] V. E. Oberacker, A. S. Umar, J. A. Maruhn, and P.-G. Reinhard, Phys. Rev. C **82**, 034603 (2010).
[42] A. S. Umar, V. E. Oberacker, J. A. Maruhn, and P.-G. Reinhard, Phys. Rev. C **80**, 041601 (2009).
[43] X. Jiang, J. A. Maruhn, and S. W. Yan, Eur. Phys. Lett. **112**, 12001 (2015).
[44] A. S. Umar and V. E. Oberacker, Phys. Rev. C **73**, 054607 (2006).
[45] E. Chabanat, P. Bonche, P. Haensel, J. Meyer, and R. Schaeffer, Nucl. Phys. A **635**, 231 (1998).
[46] A. S. Umar, M. R. Strayer, J. S. Wu, D. J. Dean, and M. C. Güçlü, Phys. Rev. C **44**, 2512 (1991).
[47] R. Keser, A. S. Umar, and V. E. Oberacker, Phys. Rev. C **85**, 044606 (2012).
[48] Kouhei Washiyama and Denis Lacroix, Phys. Rev. C **78**, 024610 (2008).
[49] V. E. Oberacker and A. S. Umar, Phys. Rev. C **87**, 034611 (2013).